Division of labor during biofilm matrix production

Anna Dragoš[1,2,7], Heiko Kiesewalter [1,8], Marivic Martin[1,2,9], Chih-Yu Hsu[3], Raimo Hartmann[4], Tobias Wechsler[5], Knut Drescher[4,6,10], Nicola Stanley-Wall[3,11], Rolf Kümmerli[5,12], Ákos T. Kovács[1,2,#,13]

[1] Bacterial Interactions and Evolution Group, Department of Biotechnology and Biomedicine, Technical University of Denmark, Kgs Lyngby, 2800, Denmark

[2] Terrestrial Biofilms Group, Institute of Microbiology, Friedrich Schiller University Jena, Jena, 07743, Germany

[3] School of Life Sciences, University of Dundee, Dundee, DD1 5EH, United Kingdom

[4] Max Planck Institute for Terrestrial Microbiology, Marburg, 35043, Germany

[5] Department of Plant and Microbial Biology, University of Zürich, Zürich, 8057, Switzerland

[6] Department of Physics, Philipps University, Marburg, 35037, Germany

Correspondence: atkovacs@dtu.dk

[#] Lead contact

[7] Twitter: @Anna_Dragos

[8] Twitter: @h_kiesewalter

[9] Twitter: @MartinMavs

[10]Twitter: @knutdrescher

[11] Twitter: @Bacteriacities

[12] Twitter: @RolfsMicrobes

[13] Twitter: @EvolvedBiofilm

Summary

Organisms as simple as bacteria can engage in complex collective actions, such as group motility and fruiting body formation. Some of these actions involve a division of labor, where phenotypically specialized clonal subpopulations, or genetically distinct lineages cooperate with each other by performing complementary tasks. Here, we combine experimental and computational approaches to investigate any benefits arising from division of labor during biofilm matrix production. We show that both phenotypic and genetic strategies for a division of labor can promote collective biofilm formation in the soil bacterium *Bacillus subtilis*. In this species, biofilm matrix consists of two major components; EPS and TasA. We observed that clonal groups of *B. subtilis* phenotypically segregate in three subpopulations composed of matrix non-producers, EPS-producers, and generalists, which produce both EPS and TasA. We further found that this incomplete phenotypic specialization was outperformed by a genetic division of labor, where two mutants, engineered as strict specialists,

complemented each other by exchanging EPS and TasA. The relative fitness of the two mutants displayed a negative frequency dependence both *in vitro* and on plant roots, with strain frequency reaching an evolutionary stable equilibrium at 30% TasA-producers, corresponding exactly to the population composition where group fitness is maximized. Using individual-based modelling, we could show that asymmetries in strain ratio can arise due to differences in the relative benefits that matrix compounds generate for the collective; and that genetic division of labor can be favored when it breaks metabolic constraints associated with the simultaneous production of two matrix components.

Key words: division of labor, biofilm, *Bacillus subtilis,* phenotypic heterogeneity, cooperation, competition, EPS, TasA

Highlights:

- matrix components EPS and TasA are costly public goods in *B. subtilis* biofilms
- genetic division of labor using Δ*eps* and Δ*tasA* fosters maximal biofilm productivity
- Δ*eps* and Δ*tasA* cooperation is evolutionary stable in laboratory and ecological systems
- costly metabolic coupling of public goods favors genetic division of labor

Introduction

Microbes can act collectively in groups, and thereby substantially influence their local environment in their own benefit. Such beneficial collective actions include the secretion of nutrient-degrading enzymes [1,2], iron-scavenging siderophores [3], biosurfactants for group motility [4,5], and structural components for biofilm formation [6,7]. In certain cases, cooperation even involves a division of labor, where subpopulations of cells specialize to perform different tasks [8–10]. For instance, during sliding colony expansion *Bacillus subtilis* cells phenotypically differentiate into surfactant producers and matrix producers where the role of the first is to reduce surface tension, while the latter allows expanding colony 'arms' to form and explore new territories [10]. Given the high relatedness between cells, specialization is likely beneficial for the group as a whole [11,12], with individuals gaining an inclusive fitness benefit from helping their clone mates [13–16]. However, division of labor has recently also been documented between genetically different strains or species [17–19].Cooperative division of labor based on genetic differentiation seems to evolve both frequently and reproducibly

[18,20], lending support for the so-called Black Queen hypothesis, which depicts the microbial world as a network of interdependencies between species [21].

While our understanding of phenotypically and genetically determined forms of division of labor in microbes deepens [10,17,18,22,23], it has remained unclear what the pros and cons of the two forms of division of labor are, and which form yields higher fitness returns for the specialists and the community as a whole. When considering division of labor based on the exchange of two beneficial public goods, a phenotypic specialization could offer advantages because cells producing the two public goods will naturally be close to one another due to binary cell division. Close spatial proximity is essential for efficient public good sharing [24,25], yet might be compromised with genetically determined division of labor, as spatial separation of partners can readily occur and the switching of specialization states is not possible [26]. Conversely, genetically determined division of labor might offer advantages because it allows a complete decoupling of traits at the metabolic level. The metabolic costs saved due to trait decoupling is likely lower in the case of phenotypic heterogeneity, because each cell might still simultaneously invest in both traits, albeit to varying extents. Finally, it has been argued that in contrast to phenotypic differentiation, terminal genetic divergence bears risks of conflicts such as social exploitation because relatedness between interacting partners is reduced; potentially leading to diverging interests between partners [26].

Here, we focus on identifying the trade-offs associated with different division of labor strategies for biofilm formation in the in the common soil and plant-colonizing bacterium *B. subtilis*, in terms of individual and population-level fitness.

Biofilms represent the most common lifestyle of bacteria, where cells are in close proximity to one another, embedded in extracellular matrix (ECM) [27]. There is ample opportunity for division of labor over matrix construction, because ECM usually consists of multiple secreted compounds that form a mesh of complex exopolysaccharides (EPS) and structural proteins, sometimes accompanied by extracellular DNA (eDNA). While the presence of eDNA can be the consequence of cell death [28], the production of matrix exopolysaccharides and proteins tends to be triggered by cooperative signaling [29,30], cues released by competitors [31], or specific nutrient components [32,33]. As the synthesis of large polymers is metabolically costly, tight regulation of matrix gene expression is often in place, and it has been suggested that the overall metabolic costs for the community may be reduced by assigning matrix production only to a subpopulation of cells [34]. Here we propose an alternative scenario involving division of labor, where subgroups of individuals within a biofilm each specialize

(either phenotypically or genetically) in the production of a different matrix component, which are then shared at the level of the group.

Our model system involves *B. subtilis* forming robust, wrinkly pellicle biofilms that reside at the oxygen rich liquid-air interface [35]. Increasing cell density of the planktonic cells results in a decreasing oxygen concentration in the bottom layers of the static medium. Aerotaxis of *B. subtilis* leads to an accumulation of cells near the liquid-air interface and eventually a colonization of the surface in a form of a densely packed pellicle biofilm. During pellicle development transcription of the matrix-related operons *epsA-O* and *tapA-sipW-tasA* is derepressed [34,36–38] eventually allowing synthesis of the biofilm exopolysaccharide (EPS), and the structural protein TasA [39,40]. Mutants lacking either EPS or TasA cannot establish pellicle biofilms individually, but they can complement each other in co-culture, indicating that both matrix components are necessary for pellicle biofilms and that they are shared [39,41,42].

Using a mixture of fitness assays, single-cell gene expression analyses and mathematical modelling, we show that the two matrix components EPS and TasA are indeed costly to produce. We further found that cells within a biofilm phenotypically differentiate into three distinct subpopulations consisting of cells producing either both of the matrix components, EPS alone, or none of the two components. We then demonstrate that in terms of group-level fitness, genetic division of labor for matrix construction is superior to the phenotypic differentiation strategy present in the wild type. Specifically, biofilm productivity was maximized at an intermediate mixing ratio of mutants deficient for either EPS or TasA, both in pellicle biofilms grown in the laboratory, and in biofilms grown on plant hosts. Crucially, the Δ*eps* : Δ*tasA* proportion at which biofilm productivity maximization occurred, represents an evolutionary stable equilibrium.

RESULTS

The matrix components EPS and TasA serve as costly public goods

Components of bacterial extracellular matrix are often large, complex polymers, which can potentially bear significant metabolic production costs [2,43–45]. To demonstrate the costs associated with the production of EPS and TasA in our *B. subtilis* strain (NCBI 3610), we competed the non-producing mutants Δ*eps* and Δ*tasA* against the wild type (WT) under conditions where matrix is synthesized but not required for survival [46], which is up to 16 hours of growth, prior to surface colonization (Movie S1; see Methods). We confirmed that in the pre-pellicle phase the WT, Δ*eps*, and Δ*tasA* strains first

grow exponentially before reaching the early stationary phase (Figure S1A), and express the corresponding matrix component (Figure S1B,C, assays based on fluorescent transcriptional reporters P_{eps}-*gfp* and P_{tapA}-*gfp*). Under these conditions, our growth competition fitness assay revealed significant costs for both matrix components (Figure 1A). The fact that Δ*eps* had significantly higher relative fitness than Δ*tasA* in pairwise competition against the WT suggests that EPS synthesis bears a higher cost than TasA production under these conditions (Figure 1A).

Next, we examined sharing of the two components. We began with complementation assays mixing the two mutants (Δ*eps* and Δ*tasA* single deletion mutants) in 1:1 ratios. In line with previous reports [39,41,42], we found that the mutants could not establish pellicles when grown in monocultures, but complemented each other when co-cultured, indicating that EPS and TasA can be shared (Figure 1B,C). Since TasA was previously depicted as a cell-associated amyloid fiber, anchored through the accessory protein TapA to the cell [41], we performed additional experiments to confirm cross-complementation. Specifically, we added conditioned media from the EPS and TasA producers to growing cultures of the Δ*eps* and Δ*tasA*, respectively, and quantified their surface colonization ability. We observed that the conditioned medium from the WT or the complementary mutant significantly improved pellicle formation as compared to the control, with the effect being more pronounced for the Δ*eps* than the Δ*tasA* mutant (Figure 1D).

As the above results (Figure 1D) suggest that the matrix components EPS and TasA differ in the extent to which they are shared, pointing towards stronger privatization of TasA, we hypothesized that efficient spatial mixing of EPS-producers and TasA-producers is necessary for successful complementation. To test the role of mixing we took advantage of a previously observed motility effect on cell assortment in pellicle biofilms [47]: Cells lacking a functional flagellum (Δ*hag*) are less efficient in swimming to the top of the liquid, which likely results in very low number of founder cells carrying the Δ*hag* mutation (compared to WT) in the pellicle. As a result, pellicles formed by two isogenic Δ*hag* strains labeled with different fluorophores, contain large clusters of cells of the same lineage, indicating limited genotype mixing [47]. As expected, the efficiency of complementation between EPS- and TasA-producers was negatively affected in the Δ*hag* genetic background as compared to the control with functional flagella (Figure S2A). Finally, the spatial assortment of cells in the pellicles formed by mixtures of Δ*eps* and Δ*tasA* and pellicles formed by the WT were compared using a density correlation function quantification method (see Methods), to assess the spatial effects of genetic division of labor (Figure S2B-D). The level of spatial strain mixing was slightly higher in

174 pellicles formed by mixtures of Δ*eps* and Δ*tasA* (regardless of the fluorescence reporter combination)
175 as compared to pellicles formed by the WT (Figure S2C,D).
176
177 Altogether, these results confirm that both matrix components EPS and TasA can be shared and that
178 robust pellicle biofilm formation depends on the efficient exchange of these compounds.
179
180 **Wild type cells exhibit phenotypic heterogeneity in the expression of matrix components**
181 As EPS and TasA are costly to produce (Figure 1A) and can both be shared between the producers and
182 non-producers (Figure 1B-D), we hypothesized that phenotypic differentiation into EPS-producers and
183 TasA-producers could occur and form the basis of a division of labor in WT *B. subtilis* populations
184 during pellicle formation. To test for phenotypic heterogeneity of *eps* and *tasA* expression at the single
185 cell level, we used a reporter strain carrying a promoter fusion of the *eps* promoter to *gfp* (P_{eps}-*gfp*)
186 and an analogous reporter for the *tapA* promoter based on *mKate* (P_{tapA}-*mKate*) at two distinct
187 genomic loci (see Methods, Table S1). As a control, we used the P_{tapA}-*gfp* P_{tapA}-*mKate* strain (see
188 Methods, Table S1) for which no phenotypic heterogeneity and a linear correlation between the two
189 fluorescence channels was expected. Fluorescent images of mature pellicles of the WT P_{eps}-*gfp* P_{tapA}-
190 *mKate* strain and the control WT P_{tapA}-*gfp* P_{tapA}-*mKate* strain were captured using confocal laser
191 scanning microscopy (CLSM). While the control strain showed a clear spatial correlation between GFP
192 and mKate fluorescence intensities, this was not the case for the WT P_{eps}-*gfp* P_{tapA}-*mKate* strain (Figure
193 2A). Specifically, large bright clusters of strong GFP signal could be observed in locations in which there
194 was reduced mKate fluorescence, suggesting the presence of a subpopulation that is partially
195 specialized for EPS production (Figure 2A). While quantitative analysis confirmed that for the P_{tapA}-*gfp*
196 P_{tapA}-*mKate* biofilm, signal intensities from GFP and mKate channels showed strong linear correlation
197 in space, this correlation was much weaker in case of P_{eps}-*gfp* P_{tapA}-*mKate* (Figure 2B, Figure S3A).
198
199 The above experiment suggests that matrix-expressing subpopulations of WT *B. subtilis* exhibit a
200 certain degree of phenotypic differentiation into cells that produce mostly EPS and cells that produce
201 both EPS and TasA (generalists). To confirm this pattern, we analyzed single cells extracted from
202 pellicles using fluorescence-guided flow cytometry (FC). FC analyses was performed at 3 time points
203 during pellicle development (24, 48 and 72 hours) and included controls with strains carrying single
204 reporter fusions (see Methods, Table S1). These analyses revealed the presence of 3 distinct
205 subpopulations of cells: (i) matrix-OFF cells where fluorescence signals from both the P_{eps} and P_{tapA}
206 promoters were below the detection thresholds; (ii) matrix-ON cells where there was a positive linear
207 correlation of the signals from the P_{eps} and P_{tapA} promoters: (iii) EPS-ON cells, containing a fluorescent
208 signal from P_{eps}, but not from P_{tapA} (Figure 2C, Figure S3B). Differences in relative frequencies of P_{eps}-

gfp and P_{tapA}-*mKate* ON cells were not due to the use of different fluorescent reporters, as evidenced by our FC control experiments where strains carrying either a P_{tapA}-*gfp* or a P_{tapA}-*mKate* showed identical frequencies of ON cells (Figure S3C,D). Thus, our FC experiments confirmed that the expression of the two major matrix promoters P_{eps} and P_{tapA} is not perfectly correlated, which likely translates into phenotypic diversity at the level of EPS and TasA production in wild type *B. subtilis* pellicles.

Genetic division of labor yields higher biofilm productivity than phenotypic differentiation

Although the above data indicate that wild type cells differentiate into EPS-producers, generalists, and non-producers during pellicle biofilm formation, this pattern does not resemble the canonical principle of division of labor where distinct subpopulations of cells are expected to either commit completely to TasA or EPS production. The incomplete specialization could be due to regulatory constraints. For instance, it is known that the *epsA-O* and *tapA-sipW-tasA* operons share multiple regulators, suggesting that some level of parallel expression (either on or off) at the single cell level is expected [48–51].

We thus wondered whether an incomplete specialization represents a beneficial strategy or whether it can be outperformed by a genetically determined specialization, where cells are ultimately constrained in the production of either TasA or EPS. To address this question, we studied the division of labor between Δ*tasA* as the exclusive EPS-producer and Δ*eps* as the exclusive TasA producer. In a first experiment, we mixed the exclusive EPS- and TasA-producers at different ratios and examined the productivities of pellicles (Figure 3A). We found that pellicle productivity varied in response to strain frequency, and peaked at a strain ratio of approximately 30 % Δ*eps* : 70% Δ*tasA* (Figure 3A). Interestingly, the group fitness of mixtures close to this optimal ratio was significantly higher than the WT productivity, indicating that the genetic division of labor over matrix construction outperforms the native phenotypic differentiation observed in the WT (Figure 3A).

Genetic division of labor is evolutionarily stable in pellicles and on plant roots

We next asked whether such genetic division of labor, which yields the highest fitness returns at a strain ratio of approximately 30:70, is an evolutionary stable strategy or simply a transient phenomenon. To test this possibility, we competed the Δ*eps* strain against the Δ*tasA* strain across a range of frequencies (1% to 99 %), over the full cycle of pellicle growth (from inoculation until formation of robust, wrinkly pellicle after 48 hours). These competitions revealed that the relative fitness of Δ*eps* followed a negative frequency-dependent pattern: Δ*eps* outcompeted Δ*tasA* when rare, but lost the competition when common (Fig. 3B). Strikingly, the two strains showed equal

competitiveness at starting frequencies between 20% - 30% Δ*eps*, thus exactly at the strain ratio where biofilm productivity is maximized. These findings strongly suggest that, regardless of the metabolic cost imbalance between the two matrix components, stable coexistence of the EPS and TasA producers is favored in the pellicle, with strain frequency evolving towards the optimum in terms of biofilm biomass productivity (Figure 1A, Figure 3B).

To test whether stable genetic division of labor could also manifest in a relevant ecological environment, we repeated several key experiments using plant root associated biofilms. Specifically, we subjected the roots of *Arabidopsis thaliana* seedlings to colonization by the WT, or a mixture of Δ*eps* and Δ*tasA* strains at a 50:50 ratio, or monocultures of the two mutants (see Methods). Each strain carried a constitutive fluorescent reporter to allow biofilm visualization by CLSM (see methods, Table S1). In line with previous studies [52], both the WT and the mixture of Δ*eps* and Δ*tasA* strains were able to produce thick biofilms on the roots, which was not the case for the Δ*eps* and Δ*tasA* mutants grown in monocultures on the plant root (Figure 4A, Figure S4A). Analogous to the pellicles, we found that the productivity of root biofilms was significantly higher for the Δ*eps* + Δ*tasA* mixture as compared to the WT. Next, we estimated the relative frequencies of Δ*eps* and Δ*tasA* mutants in the mixed biofilm on the root, based on total pixel volumes (see methods), and found that the mutant frequency settled at the optimal ratio of 20% - 30% Δ*eps* (Figure 4B,C, Figure S4B). In contrast, the frequency remained close to 0.5:0.5 in our control mixtures of two WT strains labeled with different fluorescent reporters (Figure 4B,C). Altogether, our experiments demonstrate that the genetically hard-wired division of labor between EPS- and TasA-producers provides fitness benefits not only in pellicles, but also on plant roots.

Decoupling of metabolic constraints favors the evolution of genetic division of labor

To better understand the conditions required for genetic division of labor to evolve between EPS- and TasA-producing specialists, we used an individual-based modelling platform, specifically developed to simulate multi-strain microbial interactions [53]. The platform consisted of a two-dimensional toroidal surface measuring 100 x 100 µm. Bacteria were modeled as discs with an initial diameter of 0.5 µm. They are seeded in low numbers to their *in-silico* habitat, where they could consume resources, grow, divide, disperse, and produce public goods according to specified parameters (see methods for fitness equations).

In a first set of simulations, we seeded the habitat with wildtype (WT) bacteria that simultaneously produce two complementary public goods, representing EPS and TasA. Simulations started with eight

cells placed in the center of the landscape to mimic the early phase of pellicle formation. Cells were allowed to slowly grow at a basic growth rate (μ), and divide without the need of public goods. Cells produced diffusible public goods at a constant rate. Public goods diffused randomly, could decay or generate fitness benefits for receiver cells. While each public good generates a benefit on its own, synergistic benefits accrue to cells that encounter the two complementary public goods within a certain time frame. Simulations stopped after 10,000 time steps before populations reach stationary phase. Using this setup, we found biofilm productivity in the WT to peak with lower public good diffusion coefficients *d* (Figure S5A), indicating that reduced diffusion minimizes the loss of public goods and improves sharing. Since our experimental results suggest that there are differences between TasA and EPS in the level of sharing, and thus in the relative benefit they can generate for the pellicle population, we varied this parameter in our model, but found that it did not affect the productivity of WT pellicles (Figure S5B). Next, we implemented metabolic constraints (*f*), and observed that biofilm productivity declined whenever the cost of simultaneously producing two public goods exceeds the sum of each individual public good ($f > 1$; Figure S5C).

We then asked whether the two mutants Δ*eps* and Δ*tasA* can complement each other as observed in our empirical experiments. When seeding our landscape with different ratios of the two mutants, we found that the two strains, specializing in either TasA or EPS production, could indeed complement each other, with population-level productivity peaking at intermediate mixing ratios, for all public good diffusion coefficients tested (Figure 5A, Figure S6A). Moreover, the relative fitness of the Δ*eps* strain exhibited negative-frequency dependence (Figure 5B, Figure S6B), and the point of intersection where none of the two strains experience a relative fitness advantage occurs exactly at the fitness peak of the group. Next, we implemented the experimental observation that TasA yields lower benefits than EPS into our simulations. Successful complementation also occurred under these conditions. Overall, pellicle productivity reached higher levels and peaks shifted to lower frequencies of Δ*eps* the greater the benefit imbalances between the public goods were (Figure 5C, Figure S6C). The relative fitness of Δ*eps* again followed negative-frequency dependence with the point of intersection being exactly at the pellicle fitness peak (Figure 5D, Figure S6D). The excellent qualitative match between our experimental and theoretical findings indicates that negative-frequency dependent fitness might be a general feature of public good complementation.

Finally, we asked whether genetic division of labor between Δ*eps* and Δ*tasA* outperforms the WT strategy. However, in the absence of any metabolic constraints ($f = 1$), the WT pellicle productivity was 1714 ± 39 cells after 10,000 time steps (mean ± SE, with $d = 5$), and thus the productivity was far higher

than in any of the complementation scenarios (Figure 5). Conversely, when the WT faces metabolic constraints, we found a parameter space (f > 1.1), in which pellicle productivity of complementing strains exceeds wildtype performance (Figure 5C). Taken together, our simulations recover the key features of our experimental system, and suggest that the decoupling of metabolic constraints is the main trigger for the evolution of genetic division of labor.

DISCUSSION

Despite their unicellular simplicity, microbes can coordinate complex behaviors as a group. Some of these multicellular behaviors involve division of labor between phenotypically distinct subpopulations [10,23,54,55], or even different genetic lineages [18]. Here we deployed a combination of experiments and simulations to directly compare these two alternative cooperative strategies. By focusing on the production of two biofilm matrix components in *B. subtilis*, we found evidence for significant, yet incomplete phenotypic specialization in matrix production among clonal cells of the wild type strain. However, this strategy of phenotypic specialization was outperformed by genetic division of labor, where strains, engineered as strict specialists, settled on an evolutionary equilibrium ratio that maximized biofilm productivity. Our individual-based modeling approach captures the experimental system and reveals that metabolic decoupling of two costly traits can be the key to success for genetic specialization.

While we demonstrate that *B. subtilis* WT displays partial phenotypic differentiation at the level of matrix production, we might ask why this form of specialization is not more pronounced, especially in the context of the reported fitness benefits that can accrue from complete genetic specialization (Fig. 3A). One explanation might be that the *epsA-O* and *tapA-sipW-tasA* operons share multiple regulators, such that some level of parallel expression is inevitable [48–51]. Still, there could be certain mechanisms in place to decouple EPS and TasA production, for example a positive feedback where EPS prevents autophosphorylation of the EpsAB kinase, allowing activation of the EpsE glycosyl-transferase, thereby promoting EPS-synthesis [56]. It was also proposed that the major matrix repressor SinR, acts differently on P_{eps} and P_{tapA} promoters. Specifically, in the case of P_{eps} it directly competes with an activator RemA for the binding site upstream of the promoter, thereby serving as an anti-activator, while in case of P_{tapA} it binds simultaneously with RemA, probably serving as a repressor [51]. The opposing relationship between SinR and RemA may lead to an outburst of *epsA-O* expression in a subpopulation of cells, while *tapA-sipW-tasA* remains under tighter control of SinR.

While these regulatory mechanisms could allow for some heterogeneity in gene expression, complete specialization seems impossible.

Our findings on successful genetic division of labor between specialized strains, producing either EPS or TasA, show that strain frequency settles as a stable frequency of approximately 70:30, and not at an equal ratio, as one might naively expect. Our model suggests that the dominance of EPS-producers in biofilms may be driven by a higher relative benefit of EPS compared with TasA. We can only speculate why such an asymmetry in relative benefits of EPS and TasA might occur. Perhaps, by analogy to marine exopolysaccharides [57], EPS provides buoyancy which is required for liquid-air interface colonization (as observed during spent media complementation assay). Recent work suggests that the structural functionality of TasA fibers may directly depend on the presence of EPS in the extracellular environment [58]. The 70% : 30% population structure is stable in typical laboratory setup (pellicle biofilms) and in plant root-associated biofilms.

Although the genetic division of labor arose as the winning strategy, our study also points towards the canonical problem associated with fixed cooperation strategies: limited mixing of strains prevents efficient genetic division of labor [26]. Specifically, we found that the complementation between EPS- and TasA-producers was ineffective in experiments with flagellum-deficient strains, which exhibit a decreased level of spatial mixing, thereby reducing public good sharing and the formation of robust pellicle biofilms. Mathematical models ([59], our model) suggest that complementation is most efficient when strain mixing is high, but the diffusion of public goods is reduced, conditions that foster efficient public good exchange between neighbors and prevent losses due to diffusion. A further complication is that the goods to be exchanged might often vary in their diffusion properties. Our assays, for instance, suggest that the diffusion and sharing of TasA is rather limited compared to EPS. We argue that such low diffusion rates must be compensated by an increased spatial mixing of the cooperation partners. Therefore, in opposition to “xenophobic” mechanisms employed by microbes to avoid strangers [8,60–63], “xenophilic” strategies might be crucial for genetic division of labor [64].

In conclusion, our study offers major insights into the evolution of division of labor. First, it shows that genetic specialization can be superior over phenotypic division of labor because it enables to break metabolic and regulatory constraints prevailing in organisms that remain totipotent. Second, sophisticated genetic division of labor can occur in simple organisms such as bacteria. Finally, genetic division of labor can represent an evolutionary stable strategy, with strain frequency evolving towards an equilibrium that maximizes group fitness. It is important to note that de novo mutations may occur

in the long term and disturb the observed equilibrium. For instance, a double mutant Δ*eps*Δ*tasA*, which is deficient in both matrix components could exploit the complementing partners and derail the genetic division of labor. The task of future studies will be to experimentally test whether the reported cases of genetic division of labor are evolutionary stable in the long run.

Author Contributions

A.D. and Á.T.K. conceived the project, A.D., H.K., M.M., and C.-Y.H. performed experiments, R.H. and K.D. analyzed quantitatively the CLSM imaging data, C.-Y.H. and N.S.-W. analyzed the flow cytometry results, T.W. and R.K. performed modeling and analyzed the simulations. A.D., R.K., and Á.T.K. wrote and corrected the manuscript. All authors contributed critically to the drafts and gave final approval for publication.

Acknowledgement

This work was funded by the Deutsche Forschungsgemeinschaft (DFG) to Á.T.K. (KO4741/2.1) within the Priority Program SPP1617. A.D. was supported by a fellowship from Alexander von Humboldt foundation. R.K. was funded by the Swiss National Science Foundation (grant no. PP00P3_165835) and the European Research Council (ERC-CoG no. 681295). This work was further supported by BBSRC grant code BB/P0001335 to N.S.-W., a scholarship from BeautyHsiao Biotech. Inc to C-Y.H., the European Research Council (ERC-StG no. 716734) and the Human Frontier Science Program (CDA00084/2015-C) to K.D., and a Start-up grant from the Technical University of Denmark to Á.T.K. We acknowledge the help of Dr. Rosemary Clarke for assistance with flow cytometry which was performed at the University of Dundee.

REFERENCES

1. Wilder, C.N., Diggle, S.P., and Schuster, M. (2011). Cooperation and cheating in *Pseudomonas aeruginosa*: the roles of the *las*, *rhl* and *pqs* quorum-sensing systems. ISME J. *5*, 1332–1343.
2. Drescher, K., Nadell, C.D., Stone, H.A., Wingreen, N.S., and Bassler, B.L. (2014). Solutions to the public goods dilemma in bacterial biofilms. Curr. Biol. *24*, 50–55.
3. Harrison, F., and Buckling, A. (2009). Siderophore production and biofilm formation as linked social traits. ISME J. *3*, 632–634.
4. Xavier, J.B., Kim, W., and Foster, K.R. (2011). A molecular mechanism that stabilizes cooperative secretions in *Pseudomonas aeruginosa*. Mol. Microbiol. *79*, 166–79.

5. Pollak, S., Omer-Bendori, S., Even-Tov, E., Lipsman, V., Bareia, T., Ben-Zion, I., and Eldar, A. (2016). Facultative cheating supports the coexistence of diverse quorum-sensing alleles. Proc. Natl. Acad. Sci. U. S. A. *113*, 2152–7.

6. Boyle, K.E., Heilmann, S., van Ditmarsch, D., and Xavier, J.B. (2013). Exploiting social evolution in biofilms. Curr. Opin. Microbiol. *16*, 207–12.

7. Dragoš, A., and Kovács, Á.T. (2017). The peculiar functions of the bacterial extracellular matrix. Trends Microbiol. *25*, 257–266.

8. Velicer, G.J., and Vos, M. (2009). Sociobiology of the Myxobacteria. Annu. Rev. Microbiol. *63*, 599–623.

9. Strassmann, J.E., and Queller, D.C. (2011). Evolution of cooperation and control of cheating in a social microbe. Proc. Natl. Acad. Sci. U. S. A. *108*, 10855–62.

10. van Gestel, J., Vlamakis, H., and Kolter, R. (2015). From cell differentiation to cell collectives: Bacillus subtilis uses division of labor to migrate. PLoS Biol. *13*, e1002141.

11. West, S.A., and Cooper, G.A. (2016). Division of labour in microorganisms: an evolutionary perspective. Nat. Rev. Microbiol. *14*, 716–723.

12. Zhang, Z., Claessen, D., and Rozen, D.E. (2016). Understanding microbial divisions of labor. Front. Microbiol. *7*, 2070.

13. Hamilton, W.D. (1964). The genetical evolution of social behaviour. I. J. Theor. Biol. *7*, 1–16.

14. Gilbert, O.M., Foster, K.R., Mehdiabadi, N.J., Strassmann, J.E., and Queller, D.C. (2007). High relatedness maintains multicellular cooperation in a social amoeba by controlling cheater mutants. Proc. Natl. Acad. Sci. U. S. A. *104*, 8913–7.

15. Ackerman, J.M., and Kenrick, D.T. (2008). The costs of benefits: Help-refusals highlight key trade-offs of social life. Personal. Soc. Psychol. Rev. *12*, 118–140.

16. Refardt, D., Bergmiller, T., and Kümmerli, R. (2013). Altruism can evolve when relatedness is low: evidence from bacteria committing suicide upon phage infection. Proceedings. Biol. Sci. *280*, 20123035.

17. D'Souza, G., and Kost, C. (2016). Experimental evolution of metabolic dependency in bacteria. PLoS Genet. *12*, e1006364.

18. Kim, W., Levy, S.B., and Foster, K.R. (2016). Rapid radiation in bacteria leads to a division of labour. Nat. Commun. *7*, 10508.

19. Pande, S., and Kost, C. (2017). Bacterial unculturability and the formation of intercellular metabolic networks. Trends Microbiol. *25*, 349–361.

20. Germerodt, S., Bohl, K., Lück, A., Pande, S., Schröter, A., Kaleta, C., Schuster, S., and Kost, C. (2016). Pervasive selection for cooperative cross-feeding in bacterial communities. PLOS

Comput. Biol. *12*, e1004986.

21. Morris, J.J., Lenski, R.E., and Zinser, E.R. (2012). The Black Queen Hypothesis: evolution of dependencies through adaptive gene loss. MBio *3*, e00036–12.

22. Rossetti, V., Schirrmeister, B.E., Bernasconi, M. V., and Bagheri, H.C. (2010). The evolutionary path to terminal differentiation and division of labor in cyanobacteria. J. Theor. Biol. *262*, 23–34.

23. Mohri, K., Kiyota, Y., Kuwayama, H., and Urushihara, H. (2013). Temporal and non-permanent division of labor during sorocarp formation in the social amoeba *Acytostelium subglobosum* . Dev. Biol. *375*, 202–209.

24. Julou, T., Mora, T., Guillon, L., Croquette, V., Schalk, I.J., Bensimon, D., and Desprat, N. (2013). Cell-cell contacts confine public goods diffusion inside *Pseudomonas aeruginosa* clonal microcolonies. Proc. Natl. Acad. Sci. U. S. A. *110*, 12577–82.

25. Weigert, M., and Kümmerli, R. (2017). The physical boundaries of public goods cooperation between surface-attached bacterial cells. bioRxiv, 119032.

26. Oliveira, N.M., Niehus, R., and Foster, K.R. (2014). Evolutionary limits to cooperation in microbial communities. Proc. Natl. Acad. Sci. U. S. A. *111*, 17941–6.

27. Nadell, C.D., Xavier, J.B., and Foster, K.R. (2009). The sociobiology of biofilms. FEMS Microbiol. Rev. *33*, 206–24.

28. Jakubovics, N.S., Shields, R.C., Rajarajan, N., and Burgess, J.G. (2013). Life after death: the critical role of extracellular DNA in microbial biofilms. Lett. Appl. Microbiol. *57*, 467–475.

29. Sakuragi, Y., and Kolter, R. (2007). Quorum-sensing regulation of the biofilm matrix genes (*pel*) of *Pseudomonas aeruginosa*. J. Bacteriol. *189*, 5383–5386.

30. Waters, C.M., Lu, W., Rabinowitz, J.D., and Bassler, B.L. (2008). Quorum sensing controls biofilm formation in Vibrio cholerae through modulation of cyclic di-GMP levels and repression of vpsT. J. Bacteriol. *190*, 2527–36.

31. Oliveira, N.M., Martinez-Garcia, E., Xavier, J., Durham, W.M., Kolter, R., Kim, W., and Foster, K.R. (2015). Biofilm formation as a response to ecological competition. PLOS Biol. *13*, e1002191.

32. Shemesh, M., and Chai, Y. (2013). A combination of glycerol and manganese promotes biofilm formation in Bacillus subtilis via histidine kinase KinD signaling. J. Bacteriol. *195*, 2747–2754.

33. Marsden, A.E., Grudzinski, K., Ondrey, J.M., DeLoney-Marino, C.R., and Visick, K.L. (2017). Impact of salt and nutrient content on biofilm formation by Vibrio fischeri. PLoS One *12*, e0169521.

34. Chai, Y., Chu, F., Kolter, R., and Losick, R. (2007). Bistability and biofilm formation in *Bacillus*

subtilis. Mol. Microbiol. *67*, 254–263.

35. Branda, S.S., Gonzalez-Pastor, J.E., Ben-Yehuda, S., Losick, R., and Kolter, R. (2001). Fruiting body formation by Bacillus subtilis. Proc. Natl. Acad. Sci. U. S. A. *98*, 11621–11626.

36. Kobayashi, K. (2008). SlrR/SlrA controls the initiation of biofilm formation in *Bacillus subtilis*. Mol. Microbiol. *69*, 1399–1410.

37. Cozy, L.M., Phillips, A.M., Calvo, R.A., Bate, A.R., Hsueh, Y.-H., Bonneau, R., Eichenberger, P., and Kearns, D.B. (2012). SlrA/SinR/SlrR inhibits motility gene expression upstream of a hypersensitive and hysteretic switch at the level of σD in *Bacillus subtilis*. Mol. Microbiol. *83*, 1210–1228.

38. Kearns, D.B. (2013). You get what you select for: better swarming through more flagella. Trends Microbiol. *21*, 508–509.

39. Branda, S.S., Chu, F., Kearns, D.B., Losick, R., and Kolter, R. (2006). A major protein component of the *Bacillus subtilis* biofilm matrix. Mol. Microbiol. *59*, 1229–1238.

40. Romero, D., Vlamakis, H., Losick, R., and Kolter, R. (2011). An accessory protein required for anchoring and assembly of amyloid fibres in B. subtilis biofilms. Mol. Microbiol. *80*, 1155–1168.

41. Romero, D., Aguilar, C., Losick, R., and Kolter, R. (2010). Amyloid fibers provide structural integrity to Bacillus subtilis biofilms. Proc. Natl. Acad. Sci. U. S. A. *107*, 2230–2234.

42. Martin, M., Dragoš, A., Hölscher, T., Maróti, G., Bálint, B., Westermann, M., and Kovács, Á.T. (2017). *De novo* evolved interference competition promotes the spread of biofilm defectors. Nat. Commun. *8*, 15127.

43. van Gestel, J., Weissing, F.J., Kuipers, O.P., and Kovács, Á.T. (2014). Density of founder cells affects spatial pattern formation and cooperation in Bacillus subtilis biofilms. ISME J. *8*, 2069–79.

44. Hammerschmidt, K., Rose, C.J., Kerr, B., and Rainey, P.B. (2014). Life cycles, fitness decoupling and the evolution of multicellularity. Nature *515*, 75–79.

45. Yan, J., Nadell, C.D., Stone, H.A., Wingreen, N.S., and Bassler, B.L. (2017). Extracellular-matrix-mediated osmotic pressure drives *Vibrio cholerae* biofilm expansion and cheater exclusion. Nat. Commun. *8*, 327.

46. West, S. a, Griffin, A.S., Gardner, A., and Diggle, S.P. (2006). Social evolution theory for microorganisms. Nat. Rev. Microbiol. *4*, 597–607.

47. Hölscher, T., Bartels, B., Lin, Y.C., Gallegos-Monterrosa, R., Price-Whelan, A., Kolter, R., Dietrich, L.E., and Kovács, Á.T. (2015). Motility, chemotaxis and aerotaxis contribute to competitiveness during bacterial pellicle biofilm development. J. Mol. Biol. *427*, 3695–3708.

48. López, D., Vlamakis, H., and Kolter, R. (2009). Generation of multiple cell types in *Bacillus subtilis*. FEMS Microbiol. Rev. *33*, 152–63.

49. López, D., and Kolter, R. (2010). Extracellular signals that define distinct and coexisting cell fates in *Bacillus subtilis*. FEMS Microbiol. Rev. *34*, 134–49.

50. Diethmaier, C., Pietack, N., Gunka, K., Wrede, C., Lehnik-Habrink, M., Herzberg, C., Hubner, S., and Stulke, J. (2011). A novel factor controlling bistability in *Bacillus subtilis* : the YmdB protein affects flagellin expression and biofilm formation. J. Bacteriol. *193*, 5997–6007.

51. Winkelman, J.T., Bree, A.C., Bate, A.R., Eichenberger, P., Gourse, R.L., and Kearns, D.B. (2013). RemA is a DNA-binding protein that activates biofilm matrix gene expression in *Bacillus subtilis* . Mol. Microbiol. *88*, 984–997.

52. Beauregard, P.B., Chai, Y., Vlamakis, H., Losick, R., and Kolter, R. (2013). *Bacillus subtilis* biofilm induction by plant polysaccharides. Proc. Natl. Acad. Sci. *110*, 1621–1630.

53. Dobay, A., Bagheri, H.C., Messina, A., Kümmerli, R., and Rankin, D.J. (2014). Interaction effects of cell diffusion, cell density and public goods properties on the evolution of cooperation in digital microbes. J. Evol. Biol. *27*, 1869–1877.

54. O'Connor, K.A., and Zusman, D.R. (1991). Development in *Myxococcus xanthus* involves differentiation into two cell types, peripheral rods and spores. J. Bacteriol. *173*, 3318–33.

55. Lowery, N.V., McNally, L., Ratcliff, W.C., and Brown, S.P. (2017). Division of labor, bet hedging, and the evolution of mixed biofilm investment strategies. MBio *8*.

56. Elsholz, A.K.W., Wacker, S.A., and Losick, R. (2014). Self-regulation of exopolysaccharide production in *Bacillus subtilis* by a tyrosine kinase. Genes Dev. *28*, 1710–1720.

57. Krembs, C., and Engel, A. (2001). Abundance and variability of microorganisms and transparent exopolymer particles across the ice-water interface of melting first-year sea ice in the Laptev Sea (Arctic). Mar. Biol. *138*, 173–185.

58. Erskine, E., Morris, R., Schor, M., Earl, C., Gillespie, R.M.C., Bromley, K., Sukhodub, T., Clark, L., Fyfe, P., Serpell, L., *et al.* (2017). Formation of functional, non-amyloidogenic fibres by recombinant *Bacillus subtilis* TasA. bioRxiv, 188995.

59. Allen, B., Gore, J., and Nowak, M.A. (2013). Spatial dilemmas of diffusible public goods. Elife *2*, e01169.

60. Alteri, C.J., Himpsl, S.D., Pickens, S.R., Lindner, J.R., Zora, J.S., Miller, J.E., Arno, P.D., Straight, S.W., and Mobley, H.L.T. (2013). Multicellular bacteria deploy the type VI secretion system to preemptively strike neighboring cells. PLoS Pathog. *9*, e1003608.

61. Štefanič, P., Kraigher, B., Lyons, N.A., Kolter, R., and Mandić-Mulec, I. (2015). Kin discrimination between sympatric *Bacillus subtilis* isolates. Proc. Natl. Acad. Sci. *112*, 14042–

14047.

62. Rendueles, O., Zee, P.C., Dinkelacker, I., Amherd, M., Wielgoss, S., and Velicer, G.J. (2015). Rapid and widespread *de novo* evolution of kin discrimination. Proc. Natl. Acad. Sci. U. S. A. *112*, 9076–81.

63. Lyons, N.A., Kraigher, B., Štefanič, P., Mandić-Mulec, I., and Kolter, R. (2016). A combinatorial kin discrimination system in *Bacillus subtilis*. Curr. Biol. *26*, 733–742.

64. Samad, T., Billings, N., Birjiniuk, A., Crouzier, T., Doyle, P.S., and Ribbeck, K. (2017). Swimming bacteria promote dispersal of non-motile staphylococcal species. ISME J. *11*, 1933–1937.

65. Mhatre, E., Sundaram, A., Hölscher, T., Mühlstädt, M., Bossert, J., and Kovács, Á.T. (2017). Presence of calcium lowers the expansion of *Bacillus subtilis* colony biofilms. Microorganisms *5*, 7.

66. Dragoš, A., Lakshmanan, N., Martin, M., Horváth, B., Maróti, G., García, C.F., Lieleg, O., and Kovács, Á.T. (2017). Evolution of exploitative interactions during diversification in *Bacillus subtilis* biofilms. FEMS Microbiol. Ecol.

67. Rubinstein, S.M., Kolodkin-Gal, I., Mcloon, A., Chai, L., Kolter, R., Losick, R., and Weitz, D.A. (2012). Osmotic pressure can regulate matrix gene expression in *Bacillus subtilis* . Mol. Microbiol. *86*, 426–436.

68. Shemesh, M., Kolter, R., and Losick, R. (2010). The biocide chlorine dioxide stimulates biofilm formation in *Bacillus subtilis* by activation of the histidine kinase KinC. J. Bacteriol. *192*, 6352–6.

69. Hölscher, T., Dragoš, A., Gallegos-Monterrosa, R., Martin, M., Mhatre, E., Richter, A., and Kovács, Á.T. (2016). Monitoring spatial segregation in surface colonizing microbial populations. J. Vis. Exp.

70. Konkol, M.A., Blair, K.M., and Kearns, D.B. (2013). Plasmid-encoded ComI inhibits competence in the ancestral 3610 strain of *Bacillus subtilis*. J. Bacteriol. *195*, 4085–4093.

71. Schindelin, J., Arganda-Carreras, I., Frise, E., Kaynig, V., Longair, M., Pietzsch, T., Preibisch, S., Rueden, C., Saalfeld, S., Schmid, B., *et al.* (2012). Fiji: an open-source platform for biological-image analysis. Nat. Methods *9*, 676–682.

72. López, D., Vlamakis, H., Losick, R., and Kolter, R. (2009). Paracrine signaling in a bacterium. Genes Dev. *23*, 1631–8.

73. Murray, E.J., Strauch, M.A., and Stanley-Wall, N.R. (2009). X Is involved in controlling *Bacillus subtilis* biofilm architecture through the AbrB homologue Abh. J. Bacteriol. *191*, 6822–6832.

585 **FIGURE LEGENDS**

586

587 Figure 1. **Costs and benefits of matrix components EPS and TasA. (A)** To estimate the metabolic costs
588 of EPS and TasA production the matrix-deficient strains Δ*eps* and Δ*tasA* were competed against the
589 WT and against each other under conditions where matrix components are produced but not required
590 (see Methods). Relative fitness (W) was calculated for Δ*eps* (when competed against WT), Δ*tasA*
591 (when competed against WT), and Δ*eps* (when competed against Δ*tasA*). Relative fitness W
592 significantly larger than 1 indicates an advantage of a given strain in a given pair-wise competition. For
593 Δ*eps* vs WT n=13, p<003; for Δ*tasA* vs WT n=13, p<008; for Δ*tasA* vs WT n=8, p<007 (**p<0.01, ***
594 p<0.001). **(B)** Productivity of the WT, Δ*eps*, Δ*tasA* and Δ*eps*+Δ*tasA* co-culture (50:50 ratio) measured
595 as CFU/ml. Data points represent mean and error bars represent standard error obtained from
596 biological triplicates. **(C)** Brightfield images of pellicle morphology developed by the WT, matrix-
597 deficient mutants in monocultures and by the Δ*eps*+Δ*tasA* co-culture (50:50 ratio). The cartoons below
598 represent public goods produced by each culture. **(D)** To confirm that EPS and TasA can be shared and
599 thereby serve as public goods, the matrix-deficient strains Δ*eps* and Δ*tasA* were allowed to form
600 pellicles in presence of spent media (SM) obtained from the WT or from the complementary mutant
601 (n=4-6). Pellicle productivity [CFU/ml] reached in presence of those SMs was compared with the
602 productivity of the control (a strain exposed to its own SM): for Δ*eps* + SM of WT $p<5x10^{-7}$; Δ*eps* + SM
603 of Δ*tasA* p<0.008; Δ*tasA* + SM of WT p<; Δ*tasA* + SM of Δ*eps* SM p<0.001 (**p<0.01). Boxes represent
604 Q1–Q3 (quartiles), lines represent the median, and bars span from max to min. To better distinguish
605 between the matrix-deficient mutants, data for Δ*eps* and Δ*tasA* are presented in pink and blue,
606 respectively.

607

608 Figure 2. **Native phenotypic heterogeneity in the expression of matrix components. (A)** Pellicles
609 formed by the double-labelled strain carrying the P_{eps}-*gfp* P_{tapA}-*mKate* reporters and the strain carrying
610 the P_{tapA}-*gfp* P_{tapA}-*mKate* reporters (control) were visualized using a confocal microscope to compare
611 the distribution of fluorescence signal from different fluorescence reporters (GFP, mKate). **(B)**
612 Volumes in GFP and mKate fluorescence channels (obtained by manual thresholding) were merged,
613 dissected into cubes and the average intensities in the GFP and mKate channels for all cubes were
614 plotted (see Methods). The maximum density is normalized to 1 and the contour lines correspond to
615 0.05 decrease in density. **(C)** The following strains: NCIB3610, NRS2242 (carrying P_{eps}-*gfp*), NRS3913
616 (carrying P_{tapA}-*mKate*), and NRS5832 (carrying P_{eps}-*gfp* and P_{tapA}-*mKate*); were allowed to form pellicles
617 and were then analyzed using flow cytometry. Bar chart (mean±SD) represents fraction of OFF cells,
618 cells expressing *eps-gfp*, *tapA-mKate*, and cells expressing both reporters (n=3).

Figure 3. **Productivity and fitness in pellicles with genetic division of labor. (A)** Productivities of Δ*eps*+Δ*tasA* biofilms [CFU/ml] measured for different mixing ratios and compared to average productivity reached by the WT (black horizontal line with grey shaded 95 % confidence interval). The dashed line and green shaded 95% CI represent a cubic fit to the fitness data ($F_{3, 68} = 54.9$, $R^2 = 0.695$, $p < 0.0001$). **(B)** The relative fitness of Δ*eps* in competition with Δ*tasA* followed a negative-frequency dependent trajectory, best described by a cubic fit (dashed line with 95 % CI: $F_{3,46} = 94.7$, $R^2 = 0.852$, $p < 0.0001$).

Figure 4. **Genetic division of labor on plant roots. (A)** *Arabidopsis thaliana* roots were colonized by the WT, Δ*eps*+Δ*tasA* mix and the mutants in monocultures and biofilm productivities were measured as CFU/mm of root (for WT and co-culture n=6; for Δ*eps* and Δ*tasA* n=11) (see Methods). The productivity reached by the Δ*eps*+Δ*tasA* mixture was compared with productivity of the WT ($p<0.04$). **(B)** *A. thaliana* roots were colonized by mixed cultures of WT_{GFP}+WT_{mKate} and Δeps_{GFP}+$\Delta tasA_{mKate}$ and visualized using CLSM. Scale bar represents 10µm. **(C)** Frequencies of each strain in the root-associated biofilm were determined based on image analysis (see Methods). Bars represent average (n=3-5) and error bars represent standard error.

Figure 5. **Individual-based simulations identify drivers of genetic division of labor.** We simulated biofilm formation of the mutants Δ*eps* (producing TasA) and Δ*tasA* (producing EPS). Biofilms were initiated with eight cells, with Δ*eps* frequency varying between 0 and 1, in steps of 0.125. Cells produced diffusible matrix components (either TasA or EPS) and grew according to their fitness functions. After 10,000 time steps, we measured the absolute productivity of the biofilm (no. of cells) and the relative fitness of the competing strains within biofilms. Fitness trajectories are shown as the best fit from linear models across 50 simulations for each condition (± 95 % confidence interval). **(A)** and **(B)** depict variation in biofilm productivity and relative fitness of mutants, respectively, as a function of strain frequency and the matrix diffusion coefficient, under conditions where both matrix components generate equal benefits. **(C)** and **(D)** show variation in biofilm productivity and relative fitness of mutants, respectively, as a function of strain frequency and different relative benefits of the two matrix components (diffusion coefficient $d = 5$). Dashed lines and grey shaded area in (**D**) depict mean ± 95 % CI productivities of WT biofilms across a range of metabolic constraints (f).

STAR*METHODS

CONTACT FOR REAGENT AND RESOURCE SHARING

Further information and requests for resources and reagents should be directed to and will be fulfilled by the Lead Contact, Ákos T. Kovács (atkovacs@dtu.dk).

EXPERIMENTAL MODEL AND SUBJECT DETAILS

All bacterial strains used in this study derived from *Bacillus subtilis* NCBI 3610 *comI*^{Q12l} strain (Konkol et al., 2013). Strains were maintained in LB medium (Lysogeny broth (Lennox); Carl Roth, Germany), while MSgg medium was used for pellicle formation assay [35].

METHOD DETAILS

Strain construction. All strains that were used in this study or that were used solely as gDNA donors are listed in Table S1. To obtain TB601 and TB863, the NCBI 3610 *comI*^{Q12l} was transformed with gDNA isolated from DL1032 selecting for Tet-resistant colonies or Km-resistant colonies, respectively. TB524.1 and TB525.2 were obtained by transforming TB601 with gDNA isolated from TB500.1 and TB501.1, respectively. TB538.1 and TB539.1 were obtained by transforming TB602 with gDNA isolated from TB500.1 and TB501.1, respectively. To obtain TB864 and TB865, NCBI 3610 *comI*^{Q12l} was first transformed with gDNA from 168hymKate and then with gDNA isolated from NRS2242 and NRS3913, respectively. To obtain Anc Kate P_{eps}-GFP, strain TB602 was first transformed with gDNA from 168hymKate and then with gDNA from NRS2242. To obtain Anc Kate P_{tapA}-GFP, strain TB 601 was first transformed with gDNA from 168hymKate and then with gDNA from NRS2394. In order to construct pTB848 and pTB849, the *eps* and *tapA* promoters were amplified using oTB172-oTB173 and oTB174-oTB175 primers pairs, respectively (see Table S2), the PCR products were digested with *Eco*RI and *Nhe*I, and cloned into the corresponding sites of vector pmKATErrnB. To obtain strains TB961 and TB962, first NCBI 3610 *comI*^{Q12l} was transformed with gDNA from NRS2242, and the obtained strain (TB373) was transformed with plasmids pTB848 and pTB849, respectively. TB960 was constructed by transforming NCBI 3610 *comI*^{Q12l} with gDNA from NRS3913 and the obtained strain (TB363) was subsequently transformed with pTB849 plasmid. To construct plasmid pTB498 harbouring a constitutively expressed mKATE2 gene, the $P_{hyperspank}$-mKATE2 fragment was PCR amplified with primers oTH1 and oTH2 from plasmid phy-mKATE2 [43], digested with *Xba*I and *Eco*RI, ligated into plasmid pWK-Sp as described in [65]. Resulting plasmids were verified by sequencing and transformed into *B. subtilis* NCBI 3610 *comI*^{Q12l}, resulting in TB539.

687 Plasmid pNW725 was used to construct strain NRS3913. This was generated through amplification of
688 the *mKate2* coding region from plasmid pTMN387 using primers NSW1026 and NSW1027 (see Table
689 S2) and ligation into plasmid pNW600 using *Hin*DIII and *Bam*HI. Plasmid pNW600 carries the P*tapA*
690 promoter region (Murray et al., 2009), and therefore plasmid pNW725 has the *mKate2* coding region
691 under the control of the *tapA* promoter region. Plasmid pNW725 was integrated into the chromosome
692 of *B. subtilis* NCIB3610 at the *amyE* locus. Strain NRS5832 was generated by phage transduction of the
693 P*epsA-gfp* reporter fusion from strain NRS2242 into NRS3913 as the recipient. Phage transduction was
694 performed using SSP1 phage as previously described (Verhamme et al., 2007).
695
696 ***Pellicle formation and productivity assays.*** To obtain pellicle biofilms, bacteria were routinely growth
697 in static liquid MSgg medium at 30°C for 48 hours, using 1% inoculum from overnight cultures.
698 Productivities where accessed by examining colony forming units (CFUs) in mature pellicles. Prior each
699 CFU assays, pellicles were sonicated according to a protocol optimized in our laboratory that allows
700 proper disruption of biofilms without affecting cell viability [42,66]. To access relative frequencies of
701 Δ*eps* and Δ*tasA* strains, the cocultures were plated on selective antibiotics tetracycline (10µg/ml) and
702 spectinomycin (100µg/ml), respectively.
703
704 ***Fitness assays.*** Since the expression of *epsA-O* and *tapA-sipW-tasA* operons strongly depend on
705 cultivation conditions and media composition [32,52,65,67,68], we performed the competition
706 experiment for the fitness costs of EPS and TasA production under the same conditions that were later
707 used for the assays that involved pellicles. Strains of interest were premixed at 1:1 ratios based on
708 their OD_{600} values and the mixture was inoculated into MSgg medium at 1%. Cultures were grown
709 under static conditions at 30°C. CFU assays (using selective antibiotics for the Δ*eps* and Δ*tasA* strains)
710 were performed immediately after inoculation and after 16 hours of growth. The growth curves
711 obtained at the initial stage of pellicle formation were performed under standard pellicle growth
712 conditions in 96-well plates. The optical densities and GFP-fluorescence were monitored using an
713 infinite F200PRO plate reader (TECAN Group Ltd, Männedorf, Switzerland).
714
715 ***Spent media complementation assay.*** The supernatants were obtained from the WT, Δ*eps* and Δ*tasA*
716 strains grown under static conditions in MSgg medium at 30°C for 48 hours. Cells were pelleted by
717 centrifugation (5min, 8000 r.p.m.), the supernatants were sterilized using Millipore filters (0.2µm pore
718 size), and mixed in 1:1 ratio with 2 times´ concentrated MSgg medium. Surface colonization of the
719 Δ*eps* and Δ*tasA* in presence of conditioned media from the WT or complementary mutant strains were

720 compared with the negative controls where the mutants grew in presence of their own conditioned
721 media.
722
723 ***Microscopy/confocal laser scanning microscopy (CLSM).*** Bright field images of whole pellicles and
724 colonies were obtained with an Axio Zoom V16 stereomicroscope (Carl Zeiss, Jena, Germany)
725 equipped with a Zeiss CL 9000 LED light source and an AxioCam MRm monochrome camera (Carl
726 Zeiss). For time-lapse experiment, cultures were grown in 24-well plates (1.5 cm diameter per well),
727 incubated in INUL-MS2-F1 incubator (Tokai Hit, Shizuoka, Japan) at 30 °C and images were recorded
728 every 15 min. The detailed description of the fluorescence time lapse microscope has been previously
729 published [69]. The pellicles were also analyzed using a confocal laser scanning microscope (LSM 780
730 equipped with an argon laser, Carl Zeiss) and Plan-Apochromat/1.4 Oil DIC M27 63× objective.
731 Fluorescent reporter excitation was performed with the argon laser at 488 nm and the emitted
732 fluorescence was recorded at 484–536 nm and 567–654 nm for GFP and mKate, respectively. To
733 generate pellicle images, Z-stack series with 1 µm steps were acquired. Zen 2012 Software (Carl Zeiss)
734 was used for both stereomicroscopy and CLSM image visualization.
735
736 ***Sample fixing and flow cytometry.*** Pellicles were harvested at 24, 48, and 72 h into sterile 2 ml screw
737 cap tubes, followed by centrifugation at 17000´g for 10 min. GTA buffer (50 mM glucose, 10 mM EDTA
738 pH 8.0, and 20 mM Tris-HCl pH 8.0) was added into 24-well plates to harvest the cells remained in
739 wells and pooled with cell pellet from previous step. Pooled cell pellets were then pumped through
740 23G needles 6 times to disperse pellicles. Dispersed samples were pelleted down and fixed by
741 incubation with 4% paraformaldehyde for 7 min at room temperature. Fixed samples were washed
742 with GTA, and subjected to mild sonication prior flow cytometry. Flow cytometry (LSRFortessa™, BD
743 biosciences) were operated by FACS facility in School of Life Sciences, University of Dundee.
744
745 ***Root colonization assay/root biofilms productivity.*** Colonization of *Arabidopsis thaliana* roots was
746 performed according to modified protocol from [52]. Arabidopsis ecotype Col-0 seeds were surface
747 sterilized using 2% (v/v) sodium hypochlorite solution as follows: seeds were incubated in 2% (v/v)
748 sodium hypochlorite with mixing on an orbital shaker for 20 min and then washed five times with
749 sterile distilled water. The seeds were placed on pre-dried MS agar plates (Murashige and Skoog basal
750 salts mixture; Sigma) (2.2 g l^{-1}) in an arrangement approximately 20 seeds per plate at a minimum
751 distance of 1 cm. Seeds were germinated and grown on agar plates containing MS medium. After 3
752 days of incubation at 4°C, plates were placed at an angle of 65° in a plant chamber (21°C, 16h light per
753 day). After 6 days, homogenous seedlings ranging 0.8-1.2cm in length were selected for root

colonization assay. Seedlings were transferred into 48-well plates containing 270µl of MSNg medium [52]per well. Next the medium was supplemented with 30µl of exponentially growing bacterial culture diluted to OD_{650} = 0.2. The sealed plates were incubated at rotary shaker at 28°C for 18h at 90 r.p.m. After the incubation, plants were washed 3 times with MSNg to remove non-attaching cells and then transferred to a glass slide for imaging using CLSM. To access root biofilm productivities, the roots were transferred into Eppendorf tubes, subjected to standard sonication protocol and the CFU assays were performed for obtained cell suspensions. To extract CFU/mm of root, the obtain CFU values were divided by total length of a corresponding root.

Images of plant roots. For biofilm roots visualization, the GFP and mKate images were converted into 3D projections, contrast was enhanced using normalized function and green and red lookup tables were applied for GFP and mKate channels, respectively. Overlay images were obtained in ZEN software and further processed using ImageJ as follows: Brightness and contrast were adjusted, the root and biofilm area was manually selected and the background was lightened and smoothed using 'adjust brightness' and 'smooth' functions, respectively.

Modelling. We performed individual-based simulations, using the platform developed by Dobay et al. (2014). Microbial simulations occur on a two-dimensional toroidal surface with connected edges (i.e. there are no boundaries). The surface of the torus is 10,000 μm^2 (100 x 100 µm). Bacteria are modeled as discs with an initial diameter of 0.5 µm. Bacteria can consume resources, grow at a basic growth rate (µ = 1) and divide when reaching the threshold diameter of 1 µm. In our simulations, we assumed that resources are not limited. Bacteria further produce beneficial public goods at a cost c per molecule and at constant rate of 1 molecule/s. Public goods diffuse randomly according to the diffusion coefficient d (μm^2/s) and following a Gaussian random walk. Public goods can decay with a certain probability p, with p increasing exponentially with time following the exponential function $p = 1 - e^{-w\Delta t/\partial}$, where Δt is the age of the molecule, w the stiffness of the decay and ∂ the durability of the molecule. Crucially, a public good can generate a benefit b to the cell that takes it up, which occurs when the cell and the public good physically overlap on the landscape. Bacteria can randomly disperse, too, defined by the diffusion coefficient D (μm^2/s). Because we aimed to model bacterial performance in biofilms, where cell dispersal is low, we set D = 0.01 μm^2/s. Important to note is that neither bacteria nor public goods are bound to a grid, but move on a continuous landscape (following an off-lattice model with double-precision numbers). This mimics natural bacterial behavior as close as possible, but it also leads to cells overlapping with each other. To cope with this issue, we applied an overlap correction after each time step following the procedure described by [53].

Using this setup, we simulated the performance of a wildtype (WT) strain, producing two public goods representing EPS and TasA, and two strains (PG1 and PG2) producing only one of the two public goods. We arbitrarily considered PG1 = TasA producer and PG2 = EPS producer. The growth of the three strains is defined by the following recursive functions:

$$G_{WT}(t+1) = [\mu - f(c_1 + c_2) + b_1 \sum pg1 + b_2 \sum pg2 + b_3\left(\sum pg1 + R_{pg1}\right)\left(\sum pg2 + R_{pg2}\right)]G_{WT}(t) \quad (1)$$

$$G_{PG1}(t+1) = [\mu - c_1 + b_1 \sum pg1 + b_2 \sum pg2 + b_3\left(\sum pg1 + R_{pg1}\right)\left(\sum pg2 + R_{pg2}\right)]G_{PG1}(t) \quad (2)$$

$$G_{PG2}(t+1) = [\mu - c_2 + b_1 \sum pg1 + b_2 \sum pg2 + b_3\left(\sum pg1 + R_{pg1}\right)\left(\sum pg2 + R_{pg2}\right)]G_{PG2}(t) \quad (3)$$

where G is the radius increase per time step t, μ is the basic growth rate, c_1 and c_2 are the costs of producing the respective public goods, and f is the metabolic constraint factor, whereby $f > 1$ if the simultaneous production of both public goods is costlier than producing either of the public goods alone. Furthermore, while b_1 and b_2 are the benefits accruing when a respective public good is taken up multiplied by the total number of public goods consumed (*Spg1* and *Spg2*) per time step, b_3 is the synergistic benefit accruing for all the complementary public goods taken up within a certain period of time (R_{pg1} and R_{pg2}, respectively). We arbitrarily chose five time steps for R_{pg1} and R_{pg2}.

For all simulations, we seeded our in-silico landscape with eight cells placed in the center of the landscape to mimic the early phase of pellicle formation. Cells then started to produce public goods, grew and divided defined by their growth function. We let bacteria grow for 10,000 time steps in 50 independent replicates for each parameter combination. We examined three growth treatments, which included the WT strain in monoculture, the two complementary strains PG1 and PG2 in monocultures, and the two complementary strains PG1 and PG2 in mixed cultures. In the mixed cultures, we varied the starting frequency of the two strains from 1:7 (PG1 to PG2) to 7:1. For all simulations, we extracted the absolute productivity of the biofilm and the relative fitness of the competing strains within biofilms. To assess the role of public good diffusion on biofilm productivity and relative strain fitness, we varied public good diffusion from 3 to 7 $\mu m^2/s$ in steps of 0.5 $\mu m^2/s$. To take into account that the public goods TasA and EPS might generate different benefits we varied the b_1/b_2 ratio from 1/9 to 1/1. Finally, we examined the effect of metabolic constraints on WT fitness by varying f from 1 to 1.3. All parameters together with the specific values used are given in the Supplementary Table S3.

QUANTIFICATION AND STATISTICAL ANALYSIS

Relative fitness. Relative fitness W_A for strain A in competition with strain B was calculated as follows:

$$W_A = [\ln(CFU_{A\_16h}/CFU_{A\_start})]/[\ln(CFU_{B\_16h}/CFU_{B\_start})]$$

All replicates where one strain occurred to strongly dominate in the initial inoculum (exceeding initial 0.8 frequency) were removed from the dataset.

Strain frequencies on plant roots. Ratios of the Δ*eps*^{GFP} and ΔtasA^{mKate} (and control with swapped fluorescent reporters) in root biofilms were estimated from the ratios of white pixel volumes measured on corresponding fluorescent images. Images were analyzed using ImageJ software. First, the root and biofilm area it was manually selected on the white-light image. For each channel, the stacks were converted into binary images and threshold was set up to > 0 value. Next, the root+biofilm selection was activated on the processed stacks and total pixel volumes for each channel were extracted using 'stacks statistics' function.

Density correlation. The corresponding image stacks were dissected into cubes of 10px side length. For each channel, the biovolume per cube was obtained. For all cubes containing either biovolume in either of the two fluorescence channels (designated ch1 and ch2) the total biovolume in ch1 and ch2 within a sphere of a given radius (1-5µm) was summed up, multiplied and normalized by the total volume of the sphere.

The resulting value ranges from 0 (no correlation, no biomass in one of the channels) over 0.25 (50% of biomass in ch1, 50% of biomass in ch2) to 1 (cube is filled in both channels = 100% overlap).

Statistical analysis. For relative fitness assay, statistical differences from W=1 were identified using one-sample Student's t-test. In case of productivity measurements statistical differences between two experimental groups were identified using two-tailed Student's *t*-tests assuming equal variance. Variances in the two main types of datasets (relative fitness, productivity) were similar across different samples. No statistical methods were used to predetermine sample size and the experiments were not randomized. All relevant data are available from the authors.

KEY RESOURCES TABLE

Reagent or Resource	Source	Identifier
Chemicals		

Lysogeny broth (LB), Lennox	Carl Roth GmbH	X964.1
Agar-Agar	Carl Roth GmbH	5210.3
Potassium Hydrogen Phosphate	Carl Roth GmbH	P749.1
Potassium Dihydrogen Phosphate	Carl Roth GmbH	3904.2
L-Glutamic acid Monopotassium salt monohydrate	Alfa Aesar	17232
Magnesium chloride hexahydrate	Carl Roth GmbH	2189.1
Potassium chloride	Carl Roth GmbH	6781.3
Calcium chloride	Carl Roth GmbH	5239.2
Manganese(II) chloride	Carl Roth GmbH	T881.3
Iron(III) chloride	Carl Roth GmbH	P742.1
Zinc chloride	Carl Roth GmbH	T887.1
Ammonium chloride	Carl Roth GmbH	K298.2
Thiamin	Carl Roth GmbH	T911.1
MOPS	Carl Roth GmbH	6979.4
Glycerol	Carl Roth GmbH	7533.1
Murashige and Skoog medium (MS)	Sigma Aldrich	M5519
Sodium hypochlorite	Carl Roth GmbH	9062.3
Tetracycline hydrochloride	Carl Roth GmbH	0237.1
Spectinomycin dihydrochloride	Alfa Aesar	J61820
Glucose	Fisher Scientific	G/0500/61
EDTA	VWR	20302.260
Tris	VWR	103157P
HCl	VWR	20252.335
Experimental Models: Organisms/Strains		
Bacillus subtilis NCBI 3610 *comI*^{Q12I}	[70]	DK1042
Bacillus subtilis NCBI 3610 *comI*^{Q12I} *derivatives (listed in Table S2).*	This study	N/A
Arabidopsis thaliana Col-0	Greenhouse of Max Plank Institute for Chemical Ecology, Jena	N/A
Recombinant DNA		
pmKATErrnB	[43]	Genbank Accession number: KF245454
pTB848	This study	N/A
pTB849	This study	N/A
pTB498	This study	N/A
pNW725	This study	N/A
Sequence-Based Reagents		
Primers used in this study are listed in Table S3.	This study	N/A
Software and Algorithms		
ImageJ	[71]	https://imagej.nih.gov/ij/
OriginPro 2015G	OriginLab, Northampton, MA	http://www.originlab.com/

855

856 **Supplementary Tables**

857

858 **Table S1. Bacterial strains used during experiments or as a source of genomic DNA**

Strain name	Genotype	Reference
DL1032	*eps*::*tet, tasA*::*Km, amyE*::P_{srfAA}-*lacZ (ery)*	[72]
NCIB3610	*Prototroph*	NSW laboratory
TB601	3610 *comI*^{Q12I} *eps*::*tet*	This work
TB602	3610 *comI*^{Q12I} *tasA*::*spec*	[65]
TB863	3610 *comI*^{Q12I} *tasA*::*kan*	This work
TB500	3610 *comI*^{Q12I} *amyE*::$P_{hyperspank}$-GFP (Spec^R)	[65]
TB501	3610 *comI*^{Q12I} *amyE*::$P_{hyperspank}$-mKate (Spec^R)	This work
TB524	3610 *comI*^{Q12I} *eps*::*tet amyE*::$P_{hyperspank}$-GFP (Spec^R)	This work
TB525	3610 *comI*^{Q12I} *eps*::*tet amyE*::$P_{hyperspank}$-mKate (Spec^R)	This work
TB538	3610 *comI*^{Q12I} *tasA*::*kan amyE*::$P_{hyperspank}$-GFP (Spec^R)	This work
TB539	3610 *comI*^{Q12I} *tasA*::*kan amyE*::$P_{hyperspank}$-mKate (Spec^R)	This work
168hymKate	168 *amyE*::$P_{hyperspank}$-mKATE2 (Cm^R)	[43]
TB864	3610 *comI*^{Q12I} *amyE*::$P_{hyperspank}$-mKate (Cm^R) *sacI*::P_{eps}-*gfp* (Km^R)	This work
TB865	3610 *comI*^{Q12I} *amyE*::$P_{hyperspank}$-mKate (Cm^R) *sacI*::P_{tapA}-*gfp* (Km^R)	This work
Anc Kate P_{eps}-GFP	3610 *comI*^{Q12I} *tasA*::*spec* amyE::$P_{hyperspank}$-mKate (Cm^R) *sacI*::P_{eps}-*gfp* (Km^R)	This work
Anc Kate P_{tapA}-GFP	3610 *comI*^{Q12I} *eps*::*tet* amyE::$P_{hyperspank}$-mKate (Cm^R) *sacI*::P_{tapA}-*gfp* (Km^R)	This work
TB960	3610 *comI*^{Q12I} *amyE*::P_{tapA}-*mKate* (Cm^R) *sacI*::P_{eps}-*gfp* (Km^R)	This work
TB961	3610 *comI*^{Q12I} *amyE*::P_{eps}-*mKate* (Cm^R) *sacI*::P_{tapA}-*gfp* (Km^R)	This work
TB962	3610 *comI*^{Q12I} *amyE*::P_{tapA}-*mKate* (Cm^R) *sacI*::P_{tapA}-*gfp* (Km^R)	This work
NRS2394	3610 *sacA*::P_{tapA}-*gfp* (Km^R)	[73]
NRS3913	3610 *amyE*::P_{tapA}-*mKate2* (Cm^R)	This work
NRS2242	3610 *sacI*::P_{eps}-*gfp* (Km^R)	[73]
NRS5832	3610 *sacI*::P_{eps}-*gfp* (Km^R) *amyE*::P_{tapA}-*mKate2* (Cm^R)	This work

859

860

861 **Table S2. Primers used in this study**

862

Primer	Experimental purpose	Sequence
oTB172	Cloning *eps* promoter into pmKATErrnB	CACGAATTCCAACAGCCAGCTGATTAATAG
oTB173	Cloning *eps* promoter into pmKATErrnB	CTGAGCTAGCCATTTCCTCTCCTCCTTCCCGCGGCTGGCTTC
oTB174	Cloning *tapA* promoter into pmKATErrnB	CACGAATTCCCTTCCCTCAGAGTTAAATG

oTB175	Cloning *tapA* promoter into pmKATErrnB	CTGAGCTAGCCATTTCCTCTCCTCCTGTAAAACACTGTAAC
oTH1	Cloning $P_{hyperspank}$-mKate into pWK-Sp	GCATCTAGAGTTGCTCGCGGGTAAATGTG
oTH2	Cloning $P_{hyperspank}$-mKate into pWK-Sp	CGAGAATTCATCCAGAAGCCTTGCATATC
NSW1026	Amplification *mKate2* from plasmid pTMN387	GTACAAGCTTAAGGAGGAACTACTATGGATTCAATAGAAAAGGTAAG
NSW1027	Amplification *mKate2* from plasmid pTMN387	GTACGGATCCTTATCTGTGCCCCAGTTTGCT

Table S3. Parameters and specific values used in modeling

Parameter	Description	Value(s)
μ	basic growth rate	1
D	cell diffusion	0.01
d	public good diffusion	3 - 7 $\mu m^2/s$
ω	stiffness of decay function	0.1
δ	public good durability	500 s
c_1	cost of public good 1 (TasA)	0.0005 per molecule
c_2	cost of public good 2 (EPS)	0.0005 per molecule
f	metabolic constraint factor	1 - 1.3
b_1	benefit of public good 1 (TasA)	0.0001 - 0.0009
b_2	benefit of public good 2 (EPS)	0.0001 - 0.0009
b_3	synergistic benefit	0.0005

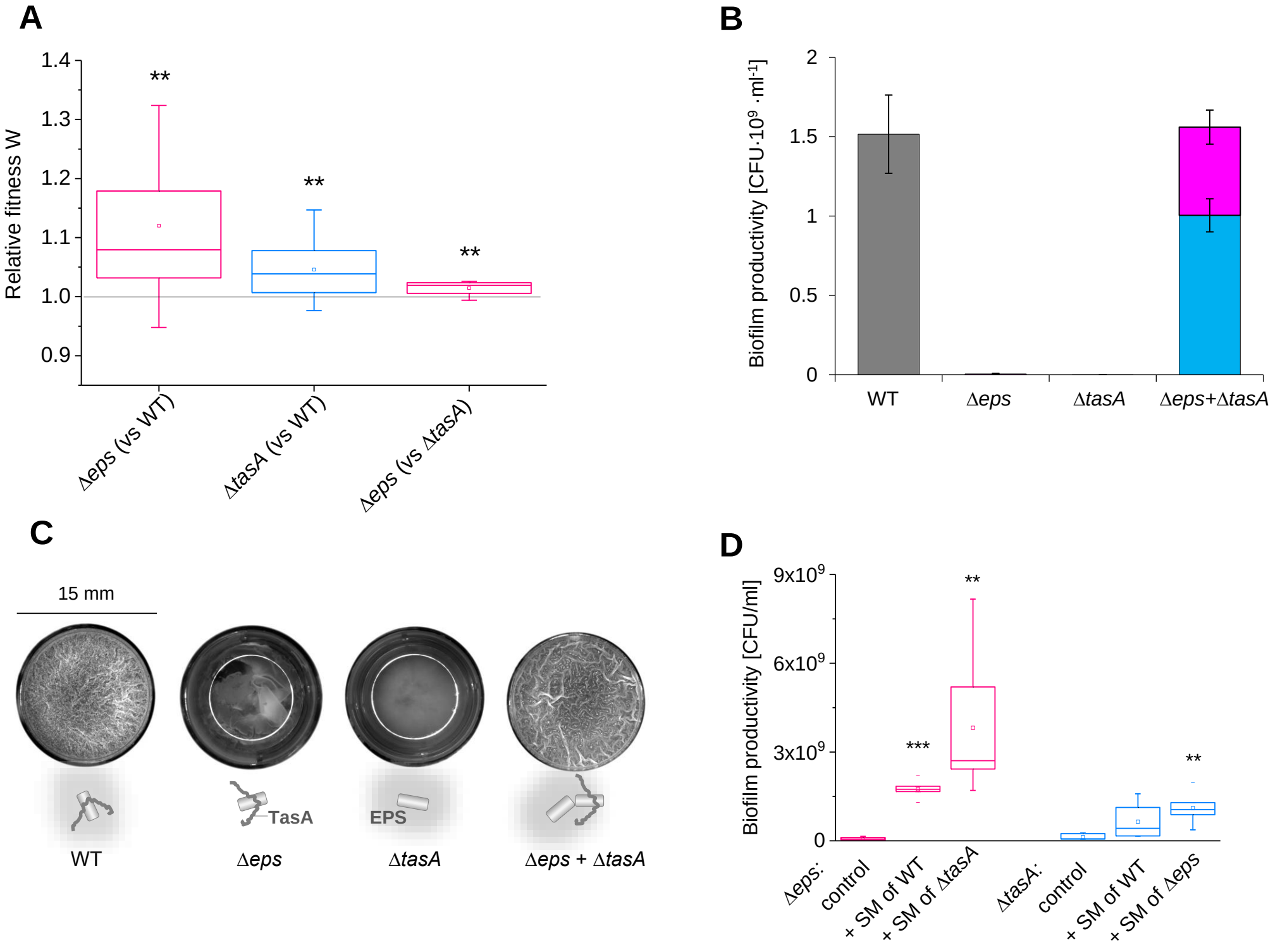
A
Relative fitness W
1.4
1.3
1.2
1.1
1.0
0.9
**
**
**
Δeps (vs WT)
ΔtasA (vs WT)
Δeps (vs ΔtasA)
B
Biofilm productivity [CFU·10⁹ ·ml⁻¹]
2
1.5
1
0.5
0
WT
Δeps
ΔtasA
Δeps+ΔtasA
C
15 mm
TasA
EPS
WT
Δeps
ΔtasA
Δeps + ΔtasA
D
Biofilm productivity [CFU/ml]
9x10⁹
6x10⁹
3x10⁹
0
***
**
**
Δeps:
control
+ SM of WT
+ SM of ΔtasA
ΔtasA:
control
+ SM of WT
+ SM of Δeps

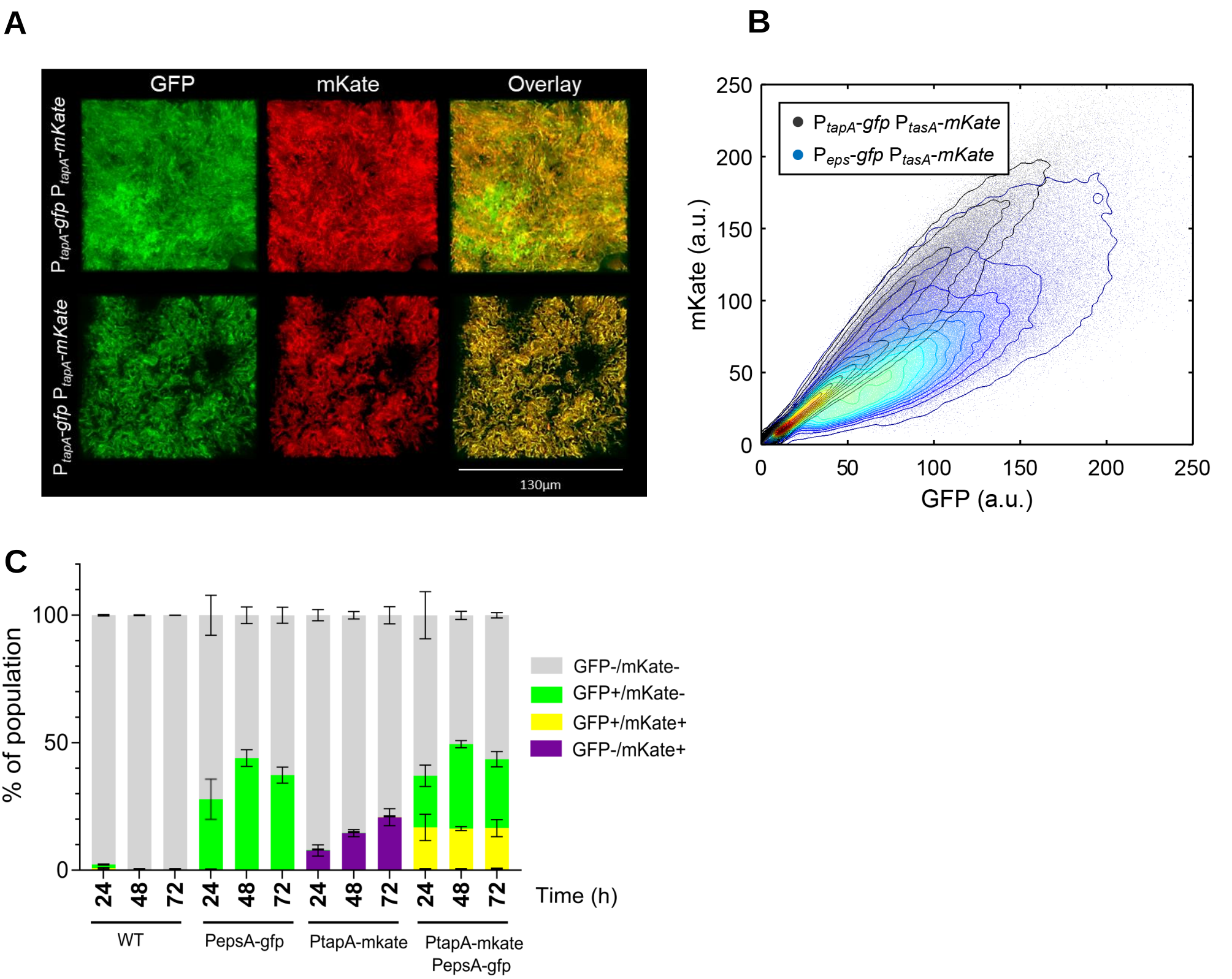
A
GFP
mKate
Overlay
P tapA-gfp P tapA-mKate
P tapA-gfp P tapA-mKate
130µm
B
P tapA-gfp P tasA-mKate
P eps-gfp P tasA-mKate
mKate (a.u.)
GFP (a.u.)
0
50
100
150
200
250
C
% of population
100
50
0
GFP-/mKate-
GFP+/mKate-
GFP+/mKate+
GFP-/mKate+
24
48
72
Time (h)
WT
PepsA-gfp
PtapA-mkate
PtapA-mkate
PepsA-gfp

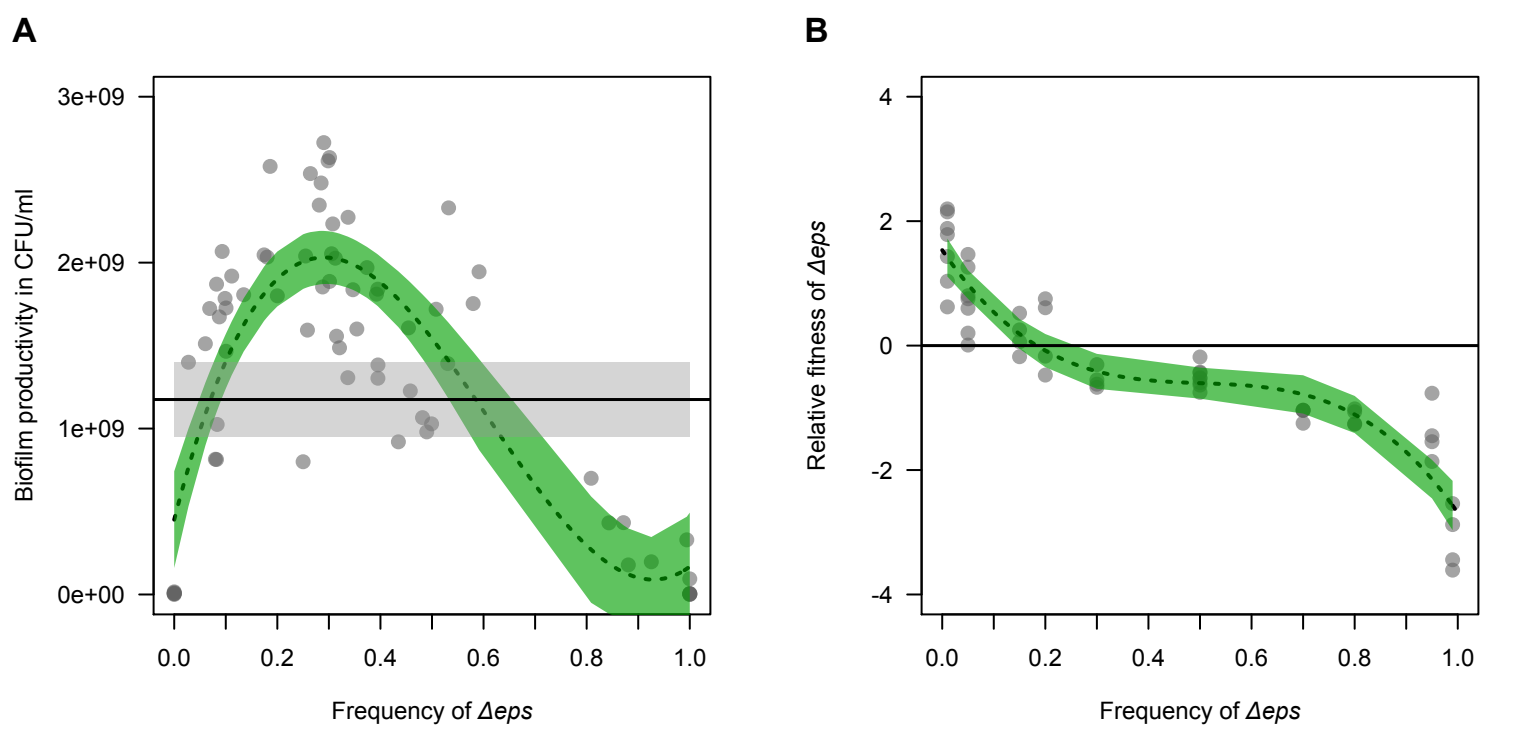
A
B
Biofilm productivity in CFU/ml
3e+09
2e+09
1e+09
0e+00
0.0
0.2
0.4
0.6
0.8
1.0
Frequency of Δeps
Relative fitness of Δeps
4
2
0
-2
-4
0.0
0.2
0.4
0.6
0.8
1.0
Frequency of Δeps

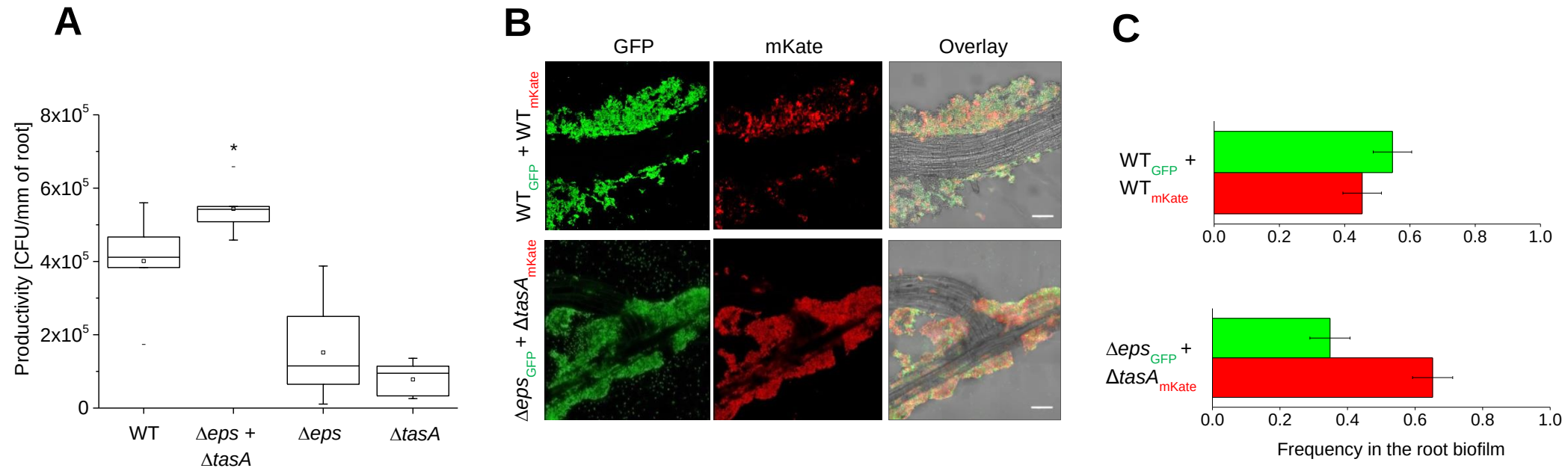
A
Productivity [CFU/mm of root]
8x10^5
6x10^5
4x10^5
2x10^5
0
WT
Δeps + ΔtasA
Δeps
ΔtasA
B
GFP
mKate
Overlay
WT GFP + WT mKate
Δeps GFP + ΔtasA mKate
C
WT GFP + WT mKate
Δeps GFP + ΔtasA mKate
0.0
0.2
0.4
0.6
0.8
1.0
Frequency in the root biofilm

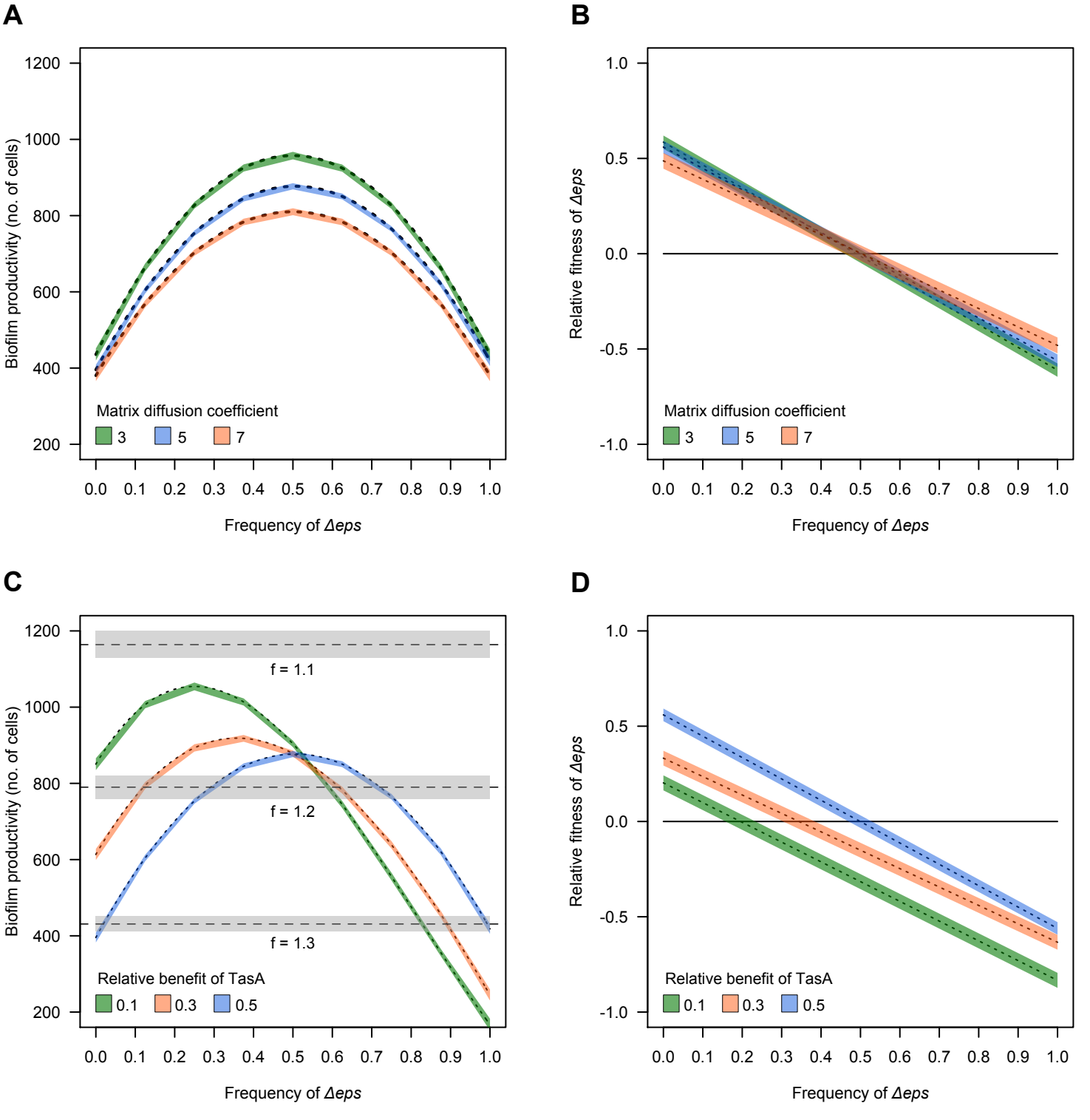
A
Biofilm productivity (no. of cells)
1200
1000
800
600
400
200
Matrix diffusion coefficient
3
5
7
0.0 0.1 0.2 0.3 0.4 0.5 0.6 0.7 0.8 0.9 1.0
Frequency of Δeps
B
Relative fitness of Δeps
1.0
0.5
0.0
-0.5
-1.0
Matrix diffusion coefficient
3
5
7
0.0 0.1 0.2 0.3 0.4 0.5 0.6 0.7 0.8 0.9 1.0
Frequency of Δeps
C
Biofilm productivity (no. of cells)
1200
1000
800
600
400
200
f = 1.1
f = 1.2
f = 1.3
Relative benefit of TasA
0.1
0.3
0.5
0.0 0.1 0.2 0.3 0.4 0.5 0.6 0.7 0.8 0.9 1.0
Frequency of Δeps
D
Relative fitness of Δeps
1.0
0.5
0.0
-0.5
-1.0
Relative benefit of TasA
0.1
0.3
0.5
0.0 0.1 0.2 0.3 0.4 0.5 0.6 0.7 0.8 0.9 1.0
Frequency of Δeps